Journal of Nuclear Materials 384 (2009) 6–11

Contents lists available at ScienceDirect

Journal of Nuclear Materials

journal homepage: www.elsevier.com/locate/jnucmat

Mechanical properties at sub-microscale and macroscale of polycrystalline uranium mononitride

Jun Adachi [a,*], Ken Kurosaki [a], Masayoshi Uno [a], Shinsuke Yamanaka [a], Masahide Takano [b], Mitsuo Akabori [b], Kazuo Minato [b]

[a] Division of Sustainable Energy and Environmental Engineering, Graduate School of Engineering, Osaka University, Yamadaoka 2-1, Suita, Osaka 565-0871, Japan
[b] Nuclear Science and Engineering Directorate, Japan Atomic Energy Agency, Tokai-mura, Naka, Ibaraki 319-1195, Japan

ARTICLE INFO

Article history:
Received 23 January 2008
Accepted 2 September 2008

PACS:
62.20.−X

ABSTRACT

The indentation hardness, Vickers hardness, fracture toughness, and Young's modulus of polycrystalline uranium mononitride (UN) at sub-microscale and macroscale were evaluated by an indentation test, Vickers hardness test, and the ultrasonic pulse echo method. The Young modulus and Vickers hardness were in good agreement with the literature values. The fracture toughness of UN was about three times that of UO_2. In addition, we revealed the indentation size effect on the indentation hardness of UN.

1. Introduction

Because of its superior properties, nitride fuel is being studied as an advanced fuel for the fast breeder reactor (FBR) [1,2] and accelerator driven system (ADS) [3,4]. For example, the superior properties are a high melting temperature, high thermal conductivity, high chemical compatibility with SUS 316 and liquid Na, and so on [5–7]. In order to evaluate the potential of nitride fuel, a lot of research has been performed to evaluate the macroscale properties of polycrystalline uranium nitride (UN). However, fission products (FP) such as the platinum family element make the microstructure of the nitride fuel complex [8–10]. Therefore, when studying the characteristics of the burnup nitride fuel, it is important to evaluate not only the macroscale properties, but also the sub-microscale properties.

The indentation test [11–13] has recently been developed, and mechanical properties such as indentation hardness and Young's modulus within sub-micron and nanoscale are widely discussed. The test is expected to be useful for measuring the mechanical properties of thin film [14,15], single crystal materials [16,17], and so on. However, there have been few studies that have applied the indentation test to nuclear fuels.

In the present study, we performed indentation tests for polycrystalline uranium mononitride (UN) to evaluate the mechanical properties of UN at the sub-microscale. For comparison, we performed the ultrasonic pulse echo measurement and Vickers hardness test. From the results of the Vickers hardness test and ultrasonic pulse echo measurement, we evaluated Vickers hardness and fracture toughness, and various elastic moduli such as Young's modulus and Poisson's ratio as the macroscale mechanical properties.

2. Experimental

The powder sample of UN was prepared from uranium dioxide (UO_2) by a carbothermic reduction. Powders of UO_2 and graphite were mixed at a molar ratio of $C/U = 2.4$. In order that the oxide phase would not remain in the product, excess graphite powder was added to the UO_2 powder. The mixed powder was heated at 1773 K under N_2 atmosphere with a flow rate of 10 l/min for 8 h, and successively heated at 1773 K under N_2 +5% H_2 atmosphere with a flow rate of 10 l/min for 8 h to remove the residual carbon. After the carbothermic reduction, the powder sample of UN was crushed by wet type ball milling using hexane for 40 h. In the ball milling, a WC ball was used. The green pellet (10 mm × φ10 mm) was obtained by the pressure under 196 MPa. The high density bulk sample of UN was sintered at 2073 K under Ar atmosphere with a flow rate of 3 l/min for 4 h and hence the bulk sample of UN was obtained. The oxygen (O_2) and carbon (C) contents were measured by an infrared absorption method, while the nitrogen (N_2) content was measured by a differential thermal conductivity method. The sample preparation and measurements of O_2, N_2 and C contents were performed in a high-purity atmosphere glove box, in which the O_2 and H_2O contents were below 10 and 40 wt. ppm, respectively.

* Corresponding author. Address: Global Nuclear Fuel-Japan Co Ltd., Engineering Service Center, Uchikawa 2-3-1, Yokosuka-shi, Kanagawa-ken 239-0836, Japan. Tel.: +81 46 833 2117; fax: +81 46 833 9249.
E-mail address: Jun.Adachi@gnf.com (J. Adachi).

0022-3115/$ - see front matter © 2008 Elsevier B.V. All rights reserved.
doi:10.1016/j.jnucmat.2008.09.019

Mechanical polishing was performed for the bulk sample using SiC polishing papers and Al_2O_3 powders, whose grain sizes were 1.0, 0.3 and 0.05 μm. Finally, chemical mechanical polishing was performed using Al_2O_3 powder with the grain size of 0.05 μm in alkaline solution (pH 9.0) to remove the surface altered layer such as the oxidation layer and strain hardening layer. The lattice parameter and crystal structure were evaluated by the X-ray diffraction (XRD) method using Cu–Kα radiation at room temperature. The bulk density of the sintered sample was determined by a geometric measurement. The area function of each grain was evaluated by the electron backscattering diffraction (EBSD) in a high vacuum (<10^{-8} Pa), and the average grain size was calculated. The surface observations were performed by a scanning electron microscope (SEM) in a high vacuum (<10^{-8} Pa) and scanning laser microscope (SLM) in air. The surface roughness was evaluated by an atomic force microscope (AFM) in air.

The longitudinal and shear sound velocities were measured by an ultrasonic pulse echo method at room temperature in air. The frequency of the transducer used in an ultrasonic pulse echo method was 5 MHz. Various elastic moduli such as Young's modulus and shear modulus can be calculated from the measured sound velocities.

Vickers hardness was measured using a Vickers hardness tester at room temperature in air. The applied load and load time were chosen to be 49, 98, 196, 490, 980, 1960, 2940 and 9800 mN, and 15 s, respectively. In the case of ceramics, fracture toughness is generally evaluated from an indentation fracture method using the length of the microcrack generated from the vertex of the Vickers indentation. However, the fracture toughness of UN had not previously been evaluated because the microcrack was scarcely generated at the Vickers indentation process, and the length of the microcrack is very short in the UN sample when the load is lower than 9800 mN. In the present study, we could observe the microcrack in the UN sample using high-resolution SLM. The fracture toughness of UN was calculated using the Niihara equation (Eq. (1)) [18]:

$$K_{IC} = 0.0181 E^{0.4} H_V^{0.6} a^{0.5} \left(\frac{C}{a} - 1\right)^{-0.5} \quad (1)$$

where E, H_V, a and C are the Young modulus, Vickers hardness, half of the diagonal length of the Vickers impression, and length of the microcrack. As the value of E, Young's modulus evaluated from the ultrasonic pulse echo method was used.

The indentation tests were performed at room temperature in air using an AFM with a nanoindenter. Details of the apparatus are reported in our previous paper [19]. Using the fused silica as the standard sample, it was confirmed that the area function [11] of the Berkovich indenter used in the present study was the same at any indentation depth. The indentation loads were chosen to be 2.0, 3.0, 4.0, 5.0, 6.0, 7.0, 10, 20, 50, 100, 200, 500, 980, and 1960 mN. In the indentation tests, the loading and unloading times were chosen to be 15 s each. From the indentation tests, the load-displacement curves of UN were obtained and include the information on the indentation depth, load and stiffness. According to the method of Oliver and Pharr [11], the indentation depth, load and stiffness enabled us to calculate the indentation hardness (H_{in}) and reduced modulus (E_r). The Young's modulus can be calculated from the following equation:

$$\frac{1}{E_r} = \frac{1 - \nu_i^2}{E_i} + \frac{1 - \nu_S^2}{E_S}, \quad (2)$$

where E and ν are the Young's modulus and Poisson's ratio, and the subscripts s and i represent the sample and indenter, respectively. Young's modulus (E_i) and Poisson's ratio (ν_i) of the diamond tip are 1140 GPa and 0.07, respectively. In the present study, Poisson's ratio calculated from an ultrasonic pulse echo method was used as the values of ν_S because the Poisson's ratio is almost independent of the porosity [20].

3. Results and discussion

3.1. Sample characteristics

Fig. 1 shows the XRD patterns of the powder sample and polished bulk sample of UN with the literature data [21]. The powder sample was obtained from part of the bulk sample before polishing. From Fig. 1, it was confirmed that the single phase of UN with a NaCl type structure was obtained in both the powder sample and bulk sample. The lattice parameters of the powder sample and bulk sample evaluated from the XRD pattern corresponded to each other, and the value was 0.4888 nm, which is consistent with the literature value (0.48897 nm) [21]. In the EBSD measurement, obvious Kikuchi patterns were observed. When there is an oxidation layer and strain hardening layer with a thickness beyond several dozen nm, the Kikuchi pattern could not be observed. From these results of XRD and EBSD, it was confirmed that there was almost no oxidation layer and strain hardening layer in the bulk sample of UN. The relative density of the bulk type sample was 92.2% of the theoretical density (%T.D.) calculated from the lattice parameter obtained from XRD analysis. From the EBSD analysis, the average grain size was 10.3 μm. From the SEM and SLM observations, the shape of the pores is nearly spherical and their sizes are approximately 1–2 μm. The sample characteristics are summarized in Table 1.

Fig. 2(a) and (b) show the indentation images of the Vickers hardness test at the load of 9800 mN and the indentation test at the load of 4.0 mN, respectively. From these figures, the indentation size obtained in the indentation test at the load of 4.0 mN is a sub-micro scale, which is remarkably smaller than the grain size. In this case, the indentation test is scarcely affected by the pore [14,22], because the plastic zone and elastic zone generated in the indentation process don't contact the grain boundaries and

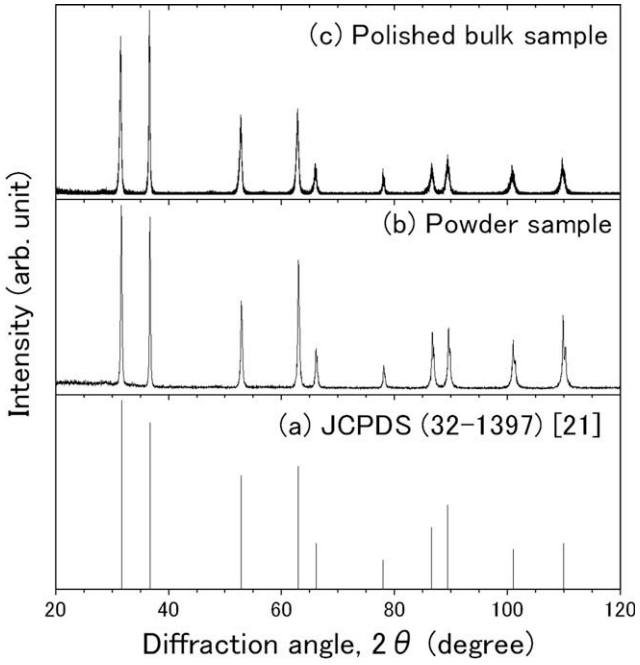

Fig. 1. XRD pattern of UN (a) literature data [21], (b) powder sample and (c) polished bulk sample.

Table 1
Sample characteristics of UN

Structure type		NaCl
Lattice parameter	nm	0.4888
Mass density	g/cm^3	13.21
Relative density	% T.D.	92.2
Grain size	μ m	17.4
N_2 content	wt%	5.68
O_2 content	wt. ppm	2464
C content	wt. ppm	938
Arithmetic average surface roughness	nm	2.4

pores. Therefore, it is assumed that the results obtained from the indentation tests at the low load represent the mechanical properties of the porosity-free materials. From the AFM analysis, the arithmetic average surface roughness of the bulk samples was detected to be below 3 nm, and its value is adequately lower than the indentation depth (>80 nm). In addition, the pile-up and sink-in [13] were not observed.

3.2. Mechanical properties

Fig. 3 shows the indentation depth h dependence of Young's modulus of UN obtained from the indentation test. In Fig. 3, Young's modulus of UN is independent of the depth in the region of $h < 1000$ nm. On the other hand, Young's modulus rapidly decreases with an increase in depth in the region of $h > 1000$ nm. The reason is that the elastic zone shown in Fig. 4 reaches the grain boundary from the depth of 1000 nm and the expansion of the elastic zone is interfered by the grain boundary. As a result, Young's modulus obtained from the indentation test becomes low. In the present study, we considered the average of Young's modulus obtained in the region of $h < 1000$ nm to be Young's modulus of porosity-free UN. The values of sound velocities and elastic moduli obtained from the ultrasonic pulse echo measurements are summarized in Table 2. Fig. 5 shows the porosity dependence of Young's modulus obtained from the ultrasonic pulse echo measurements and indentation tests, together with the literature data [23–27]. Hayes and Peddicord [23] revealed the porosity (P) and temperature (T) dependences of Young's modulus (E) of UN as the following equation:

$$E(\mathrm{MPa}) = 0.258[(1-P)\times 100]^{3.446}[1-2.375\times 10^{-5}T] \quad (0 < P < 0.3,\ 298 < T < 1473\ \mathrm{K}). \tag{3}$$

From Fig. 5, Eq. (3) is consistent with the results obtained from the ultrasonic pulse echo measurement at 92.2%T.D. and the indentation test at 100%T.D. This result proves that Young's modulus

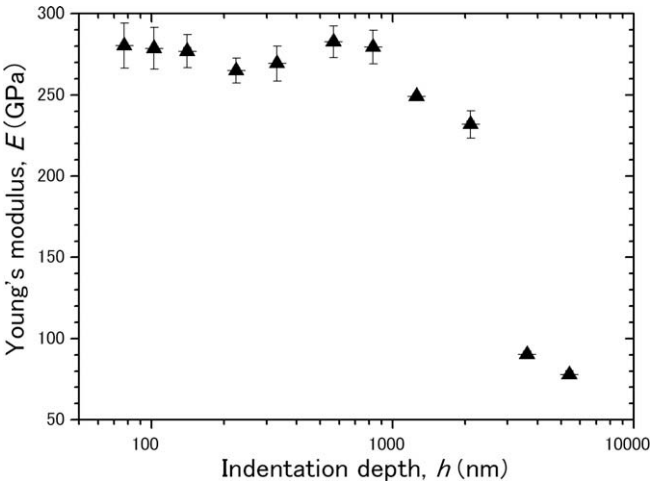

Fig. 3. Indentation depth dependence of Young's modulus of UN.

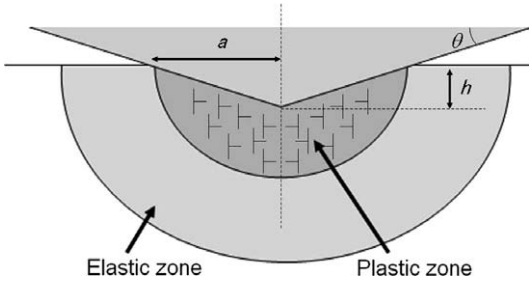

Fig. 4. Schematic of elastic and plastic zone on indentation test [13].

Table 2
Sound velocities and elastic moduli obtained by ultrasonic pulse echo measurement of UN

Longitudinal velocity, V_L	m/sec	4378
Shear velocity, V_S	m/sec	2507
Young's modulus, E	GPa	208
Shear modulus, G	GPa	83
Poisson's ratio, ν		0.256
Bulk modulus, B	GPa	142
Debye temperature, θ	K	339

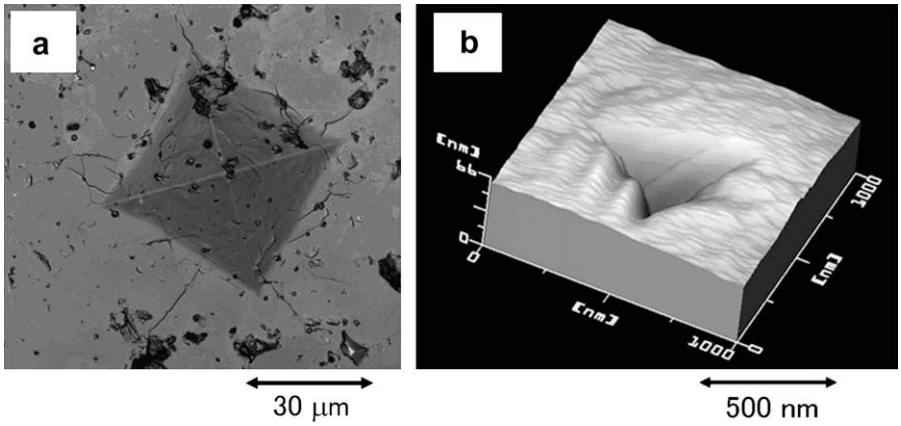

Fig. 2. Indentation image (a) Vickers hardness test at the load of 9800 mN (SLM image), (b) indentation test at the load of 4.0 mN (AFM image).

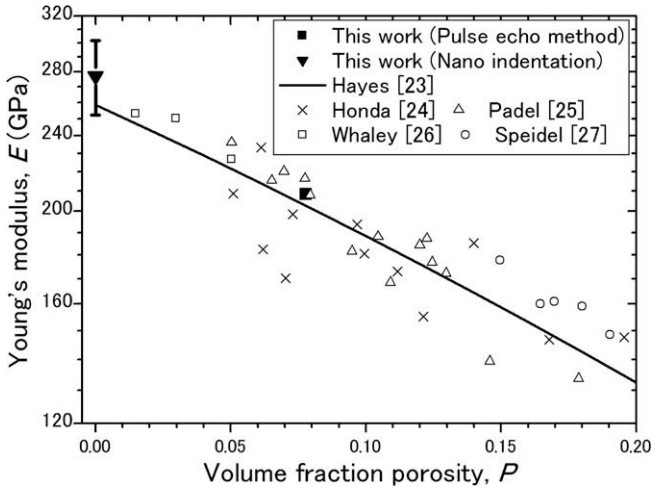

Fig. 5. Porosity dependence of Young's modulus of UN, together with the literature data [23–27].

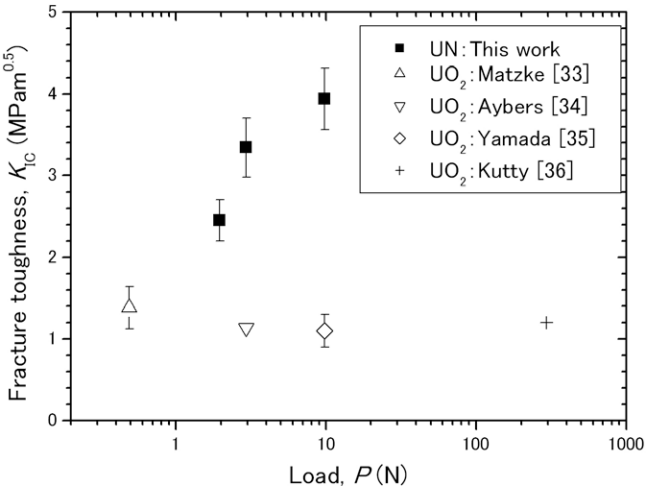

Fig. 7. Load dependence of the fracture toughness of UN, together with the literature data of UO_2 [33–36].

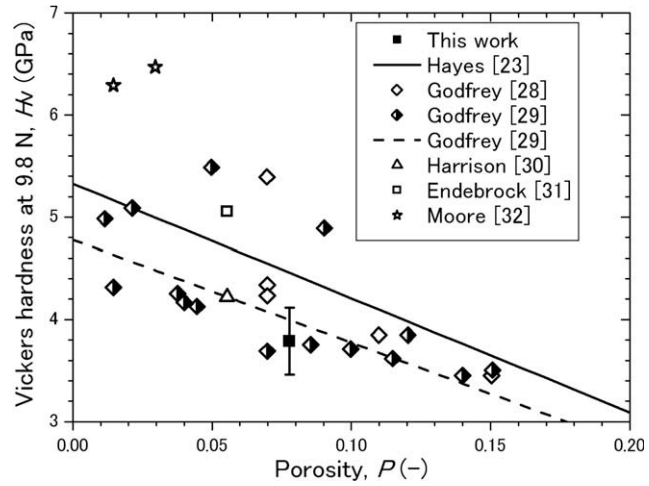

Fig. 6. Porosity dependence of Vickers hardness of UN at load of 9.8 N, together with the literature data [23,28–32].

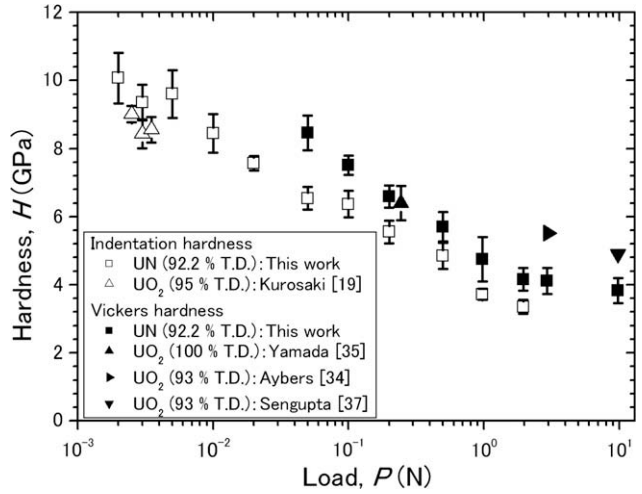

Fig. 8. Load dependence of the hardness of UN, together with the literature data of UO_2 [19,34,35,37]. In this figure, the white and black points represent the indentation hardness and Vickers hardness, respectively.

obtained from the indentation test represents the value of the porosity-free material.

Fig. 6 shows the porosity dependence of Vickers hardness at 9800 mN, together with the literature data [23,28–32]. Hayes and Peddicord [23] and Godfrey and Hallerman [29] revealed the porosity and temperature dependences of the Vickers hardness of UN as the following equation.

$$\text{Hayes}[22]: H_V(\text{GPa}) = 9.334[1-2.1P]\exp(-1.882\times10^{-3}T)\} \quad (0<P<0.26, 298<T<1673K) \tag{4}$$

$$\text{Godfrey}[29]: H_V(\text{GPa}) = 4.7778[1-2.1P] (0<P<0.26) \tag{5}$$

From Fig. 6, the Vickers hardness of UN obtained in the present study is very consistent with Eq. (5).

The load dependence of the fracture toughness of UN is shown in Fig. 7, together with the literature data of UO_2 [33–36]. In the present study, the microcrack could not be observed below the load of 980 mN. At the load of 9800 mN, the fracture toughness of UN is about three times that of UO_2. From this result, it is thought that the pellet cracking in nitride fuels resulting from the thermal stress is vastly smaller than that in oxide fuels, because the fracture toughness and thermal conductivity of UN are higher than those of UO_2.

Fig. 8 indicates the load dependence of Vickers hardness and the indentation hardness of UN, together with the literature data of UO_2 [19,34,35,37]. In this figure, both the Vickers hardness and indentation hardness decrease when the load is increased. This phenomenon is called the indentation size effect (ISE). Nix and Gao [38] formulated the ISE by the strain gradient plasticity [39] based on geometrically necessary dislocations (GNDs) [40]. In the Nix and Gao model, the ISE is represented by the following equation:

$$\left(\frac{H}{H_0}\right)^2 = 1+\frac{h_0}{h} \tag{6}$$

where H and h are the indentation hardness and depth, H_0 is the indentation hardness when the depth (h) becomes infinitely large, and h_0 is the length scale. H_0 and h_0 are generally obtained by the fitting of Eq. (6) for the experimental data. Thus, the ISE cannot be explained from the load dependence of the hardness, but can be explained from the relationship of $1/h$ and H^2. Therefore, the relationship of $1/h$ and H^2 is shown in Fig. 9. In this figure, the experimental data follows the Nix and Gao model in the region of $h > 170$ nm, but the Nix and Gao model overestimates the hardness

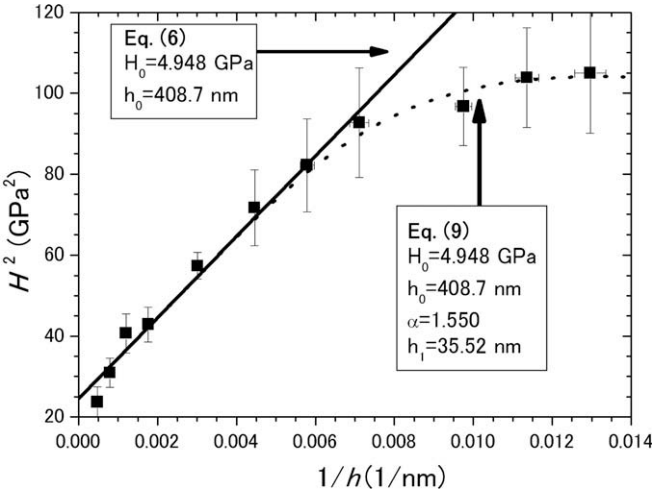

Fig. 9. Square of indentation hardness versus inverse of depth (UN).

in the region of $h < 170$ nm. In the same way, Swadener et al. [41] and Feng and Nix [42] evaluated the ISE on Ir and MgO, respectively. In the case of Ir and MgO, the Nix and Gao model also overestimated the hardness at low h. In the Nix and Gao model, it is assumed that all the GNDs are contained in a hemisphere plastic zone, with a radius equal to the contact radius a. Swadener suggested that this assumption may not be correct at low h and that GNDs spread-out from the hemisphere plastic zone with a radius equal to the contact radius a due to the repulsive force between dislocations. The spread-out effect was experimentally confirmed by Feng. Feng suggested the effective plastic zone with a radius of fa to account for the spread-out effect, and improved the Nix and Gao model as the following equation:

$$\left(\frac{H}{H_0}\right)^2 = 1 + \frac{h_0}{f^3 h}. \tag{7}$$

Feng formulated the form of function ($f(h)$) as Eq. (8):

$$f = 1 + \alpha e^{-h/h_1}, \tag{8}$$

where α and h_1 are the fitting parameters. From Eqs. (7) and (8), Eq. (9) was obtained:

$$\left(\frac{H}{H_0}\right)^2 = 1 + \left(1 + \alpha e^{-h/h_1}\right)^{-3} \frac{h_0}{h}. \tag{9}$$

The experimental data was adequately fitted by using Eq. (9), as shown in Fig. 9. From the fitting by Eq. (9), the depth dependence of the indentation hardness of UN was revealed as the following equation:

$$\left(\frac{H}{4.948}\right)^2 = 1 + \left(1 + 1.550 e^{-h/35.52}\right)^{-3} \frac{408.7}{h} \quad (70\ \text{nm} < h < 2000\ \text{nm}) \tag{10}$$

Eq. (10) allows us to estimate the indentation hardness of UN under various indentation depths and loads. In Fig. 8, the Vickers hardness of UN is smaller than that of UO_2. However, the indentation hardness of UN is larger than that of UO_2. This reason would be also the indentation size effect.

4. Summary

The bulk sample of polycrystalline UN was prepared by a carbothermic reduction and the mechanical properties of UN were evaluated at the sub-microscale and macroscale. The values of Young's modulus estimated from Hayes's equation (Eq. (3)) were very consistent with the results of the ultrasonic pulse echo method and indentation test. The Vickers hardness of UN obtained in the present study was consistent with Godfrey's equation (Eq. (5)). The fracture toughness of UN was about three times that of UO_2. The indentation hardness decreased with an increase in the load due to strain hardening resulted from the generation of geometrical necessary dislocations in the indentation process. Using the model for the indentation size effect, which was suggested by Nix and Gao and improved by Feng, the authors revealed the relationships between the indentation depth and indentation hardness as the following equation:

$$\left(\frac{H}{4.948}\right)^2 = 1 + \left(1 + 1.550 e^{-h/35.52}\right)^{-3} \frac{408.7}{h} \quad (70\ \text{nm} < h < 2000\ \text{nm})$$

By using this equation, we can estimate the indentation hardness under various indentation depths and loads. From these results, it was confirmed that the indentation test would be very useful when evaluating high-burnup fuel and cladding material, which have very complex microstructures.

Acknowledgments

The present study includes the results of 'Technological Development of a Nuclear Fuel Cycle Based on Nitride Fuel and Pyrochemical Reprocessing' entrusted to JAEA by the Ministry of Education, Culture, Sports, Science and Technology of Japan (MEXT). The sample preparation was performed in Mitsubishi Materials Co.

References

[1] H. Matzke, Science of Advanced LMFBR Fuels, Elsevier Science Publications Co, New York, USA, 1986.
[2] H. Blank, J. Nucl. Mater. 153 (1988) 171.
[3] T. Sasa, H. Oigawa, K. Tsujimoto, K. Nishihara, K. Kikuchi, Y. Kurata, S. Saito, M. Futakawa, M. Umeno, N. Ouchi, Y. Arai, K. Minato, H. Takano, Nucl. Eng. Des. 230 (2004) 209.
[4] H. Yoshida, M. Kubota, H. Katsura, M. Mizumoto, T. Mukaiyama, T. Takizuka, in: 7th Int. Conf. Emerging Nucl. Energy Syst., 1993, pp. 463–467.
[5] A.A. Bauer, P. Cybulskis, J.L. Green, Adv. LMFBR Fuels Top. Meet. Proc. (1977) 299.
[6] D. Brucklacher, Fak. Maschinenbau, Fed. Rep. Ger. Avail. INIS. Report mf-5402 (1978) 101.
[7] A.K. Sengupta, C. Ganguly, T. Indian I. Metals 43 (1990) 31.
[8] R.B. Matthews, K.M. Chidester, C.W. Hoth, R.R. Mason, R.L. Petty, J. Nucl. Mater. 151 (1988) 334.
[9] Y. Arai, A. Maeda, K. Shiozawa, T. Ohmichi, J. Nucl. Mater. 210 (1994) 161.
[10] M. Uno, K. Kurosaki, A. Nakamura, J. Nucl. Mater. 247 (1997) 322.
[11] W.C. Oliver, G.M. Pharr, J. Mater. Res. 7 (1992) 1564.
[12] S. Suresh, A.E. Giannakopoulos, J. Alcala, Acta Mater. 45 (1997) 1307.
[13] A.C. Fisher-Cripps, Nanoindentation, Springer Co, New York, USA, 2002.
[14] B.K. Jang, H. Matsubara, Mater. Lett. 59 (2005) 3462.
[15] E. Atar, C. Sarioglu, U. Demirler, E.S. Kayali, H. Cimenoglu, Scripta Mater. 48 (2003) 1331.
[16] K. Kurosaki, D. Setoyama, J. Matsunaga, S. Yamanaka, J. Alloys Compd. 386 (2005) 261.
[17] F.K. Mante, G.R. Baran, B. Lucas, Biomaterials 20 (1999) 1051.
[18] K. Niihara, R. Morena, D.P.H. Hasselman, J. Mater. Sci. Lett. 1 (1982) 13.
[19] K. Kurosaki, Y. Saito, H. Muta, M. Uno, S. Yamanaka, J. Alloys Compd. 381 (2004) 240.
[20] R.W. Rice, Porosity of ceramics, Marcel Dekker Inc, New York, USA, 1999. p. 131.
[21] JCPDS card 32-1397 (UN).
[22] R.G. Wellman, A. Dyer, J.R. Nicholls, Surf. Coat. Tech. 176 (2004) 253.
[23] S.L. Hayes, J.K. Peddicord, J. Nucl. Mater. 171 (1990) 271.
[24] T. Honda, T. Kikuchi, J. Nucl. Sci. Technol. 6 (1968) 221.
[25] A. Padel, C.D. Novion, J. Nucl. Mater. 33 (1969) 40.
[26] H.L. Whaley, R.A. Potter, W. Fulerson, US At. Energy Comm. ORNL-4370 (1968) 86.
[27] E.O. Speidel, D.L. Keller, US At. Energy Comm. BMI-1633 (1963) 65.
[28] T.G. Godfrey, G. Hallerman, O.B. Cavin, US At. Energy Comm. ORNL/TM-1050 (1965) 142.

[29] T.G. Godfrey, G. Hallerman, US At. Energy Comm. ORNL-3870 (1965) 66.
[30] J.D.L. Harrison, US At. Energy Comm. ORNL-4330 (1968) 28.
[31] R.W. Endebrock, E.L. Foster, D.L. Keller, US At. Energy Comm. BMI-1690 (1968) 22.
[32] J.P. Moore, W. Fulkerson, D.L. McElroy, J. Am. Ceram. Soc. 53 (1970) 76.
[33] H. Matzke, J. Spino, J. Nucl. Mater. 248 (1997) 170.
[34] M.T. Aybers, R. Artir, A.A. Aksit, S. Akbal, Mater. Charact. 57 (2006) 182.
[35] K. Yamada, S. Yamanaka, M. Katsura, J. Alloys Compd. 271–273 (1998) 697.
[36] T.R.G. Kutty, K.N. Chandrasekharan, J.P. Panakkal, J.K. Ghosh, J. Mater. Sci. Lett. 6 (1987) 260.
[37] A.K. Sengupta, C.B. Basak, T. Jarvis, R.K. Bhagat, V.D. Pandey, S. Majumdar, J. Nucl. Mater. 325 (2004) 141.
[38] W.D. Nix, H. Gao, J. Mech. Phys. Solids 46 (1998) 411.
[39] N.A. Fleck, J.W. Hutchinson, J. Mech. Phys. Solids 41 (1993) 1825.
[40] M.F. Ashby, Phil. Mag. 21 (1970) 399.
[41] J.G. Swadener, E.P. George, G.M. Pharr, J. Mech. Phys. Solids 50 (2002) 681.
[42] G. Feng, W.D. Nix, Scripta Mater. 51 (2004) 599.